Role of Capillarity in Penetration into and Flow Through Fibrous Barrier Materials

E. Unsal,[1] P. Schwartz,[1] J. H. Dane[2]

[1]*Department of Textile Engineering, 115 Textile Building, Auburn University, Auburn, Alabama 36849*
[2]*Department of Agronomy and Soils, Funchess Hall, Auburn University, Auburn, Alabama 36849*

Received 12 December 2003; accepted 14 July 2004
DOI 10.1002/app.21269
Published online in Wiley InterScience (www.interscience.wiley.com).

ABSTRACT: Hydrophobic fibrous media, in the form of barriers, provide protection to its user against fluids. Important aspects to consider are the pressure at which liquids (nonwetting fluids) will penetrate into the fabric and the rate at which it will flow through. At the same time we need to consider the comfort level that the fabric provides, that is, the pores should be large enough to allow the exchange of air. The objective of this study was to develop an experimental technique to determine (1) the displacement pressure of medical barrier fabrics in combination with aqueous solutions and (2) the flow rates once the aqueous solutions had penetrated. A pressure/flow cell was used to make these determinations during sequences of increasing and decreasing pressures applied to the nonwetting fluids (aqueous solution). The resulting flow rate–pressure curves exhibited hysteresis, that is, lower flow rates existed during increasing pressures (increasing liquid contact) than during decreasing pressures (decreasing liquid contact) at corresponding pressure values. The reasons for this hysteresis were investigated. The flow rate–pressure curves also provided information about the pore size distributions of the fabrics. © 2004 Wiley Periodicals, Inc. J Appl Polym Sci 95: 841–846, 2005

Key words: poly(propylene) (PP); barrier; hysteresis; reinforcement; pore size distribution

INTRODUCTION

Liquid penetration into and its subsequent flow through porous materials depend on both the molecular and bulk properties of the liquid, and the geometric and surface properties of the porous medium. Before it can move into a fibrous medium, the liquid must exceed the displacement pressure. For a hydrophilic medium, there is an attraction between the aqueous phase liquid and the solid surface. Thus, spontaneous uptake occurs. However, for a hydrophobic medium, the water molecules are being repelled and for penetration to occur the aqueous phase liquid must be forced into the medium.[1] The required displacement pressure depends on the pore sizes, the liquid surface tension, and the contact angle between the solid surface and the liquid phase.

Forced flow of fluids through fibrous materials plays an important role in a variety of applications. During manufacturing of many fiber-reinforced composites, polymeric resins must impregnate the fibrous reinforcements. In filtration processes, the porous media are designed to trap particles, gases, and biological contaminants. They can also be designed as barriers to stop contaminants from spreading. The most effective barriers are those textiles coated with impermeable films. However, when used by humans the heating and cooling of the body involves moisture transport. To keep the wearer from overheating, there must be a way to allow for moisture transport.[2] The dilemma between high protection and comfort requires a fabric that combines both properties. Fabrics such as Gortex®, SMS®, and Sontara® are able to give the necessary protection and desired comfort to their wearers.

Considerable knowledge exists regarding wetting, surface interactions between fluid and solid phases, and penetration into and flow through textile structures.[3–9] A test method was developed by Miller and Clark[5,6] for studying wetting and steady-state liquid flow through wool, cotton, and acrylic knitted fabrics; years later, Miller and Schwartz[7] developed a similar methodology to study the wetting and flow behavior of aramid and bilaminate poly(propylene) in nonwoven fabrics. Several methodologies have been developed to understand resin impregnation during composite manufacturing.[10–12] These studies dealt with the initial contact between the solid and liquid phases and the initial penetration. However, not much is known regarding flow after penetration. In this article, we present a theoretical analysis supported by experimental data, to understand better the liquid penetration into and its subsequent flow through five different barrier fabrics.

Correspondence to: P. Schwartz (schwartz@eng.auburn.edu).

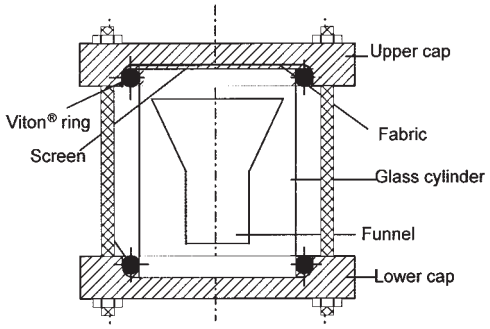

Figure 1 Pressure/flow cell.

EXPERIMENTAL

Test apparatus

A simplified diagram of the pressure/flow cell, which was used for measuring penetration/displacement pressures and flow rates, is presented Figure 1. A fabric sample was clamped between the upper end cap and the Viton® O-ring. The latter was supported by a glass cylinder, which was positioned between the upper and lower end caps. The caps were secured in place with threaded rods and nuts. The sample was supported by a rigid metal screen. The upper cap had an inlet connected to the liquid supply. The screen, which helped to minimize sagging of the sample, had openings large enough to allow air and water to pass freely through the material. The cylinder inside diameter was 80 mm and its height was 100 mm. The displacing fluid was placed in a glass reservoir with a volume of 8000 cm^3 (Fig. 2). The top of the reservoir was connected to an air pressure source to provide the required air pressure to the displacing liquid. The opening at the bottom of the reservoir was connected to the inlet of the upper cap of the pressure/flow cell.

When the sample is clamped between the screen and the O-ring, some damage might occur at the edges of the fabric, if not at the time of clamping, than during flow, especially under high pressures. To avoid inaccuracies in the flow results, a glass funnel with a diameter smaller than the glass cylinder was placed under the fabric to eliminate collecting liquid from the edges of the fabric. The funnel diameter was 65 mm at the top.

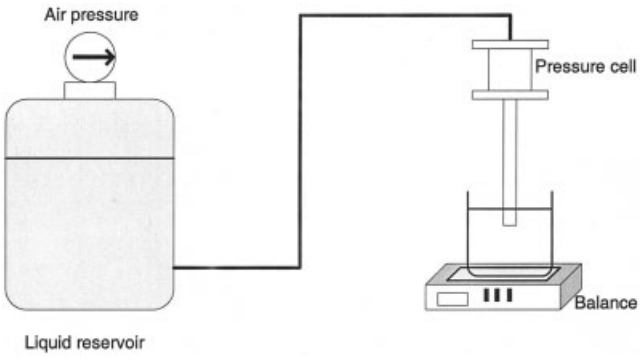

Figure 2 Cross-sectional view of test setup.

TABLE I
Fabric Properties[a]

Fabric	Thickness (μm)	Smallest pore size (μm)	Biggest pore size (μm)	Average pore size (μm)
A	0.36 [0.012]	7.88 [1.38]	14.48 [0.36]	8.38 [1.11]
B	0.36 [0.013]	11.62 [3.52]	25.00 [3.70]	13.80 [1.19]
C	0.29 [0.006]	15.55 [2.00]	36.66 [6.00]	30.00 [5.00]
D	0.46 [0.013]	14.46 [1.16]	33.69 [0.62]	17.77 [0.77]
E	0.36 [0.031]	12.87 [2.02]	36.77 [2.53]	19.22 [1.75]

[a] Standard deviation in square brackets.

Materials

Five barrier fabrics, hereafter referred to as A, B, C, D, and E, were tested. Fabics A and B (provided by Kimberley Clark, Roswell, GA) were made of 100% poly(propylene) (PP) materials, commonly used for protective medical garments, especially for surgical gowns and drapes. Fabric C was a medical Sontara®, provided by DuPont (Wilmington, DE) and made of polyester and wood pulp fibers. Fabrics D and E, also used for surgical gowns, drapes, and leggings, were provided by BBA Nonwovens Inc. (Simpsonville, SC) and consisted of 100% PP materials. Fabric properties are given in Table I.

Fabric thickness was determined using a digital micrometer (TMI, Ronkonkoma, NY) following the guideline of ASTM D1777 Standard.[14] Pore size distributions were determined with a capillary flow porometer (Porous Materials, Inc., Ithaca, NY). Scanning electron microscope (SEM) images were obtained for all samples before (Fig. 3–7) and after each fluid pen-

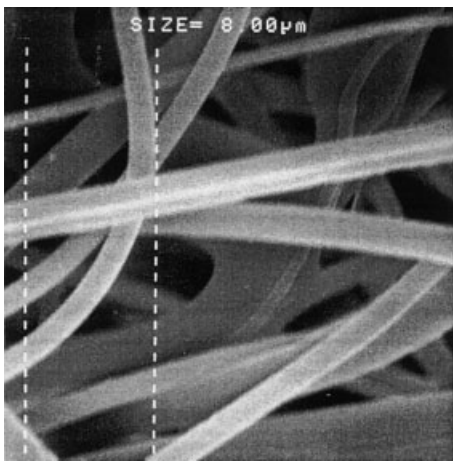

Figure 3 SEM image of Sample A (10 kV, 14 mmWD, ×3000).

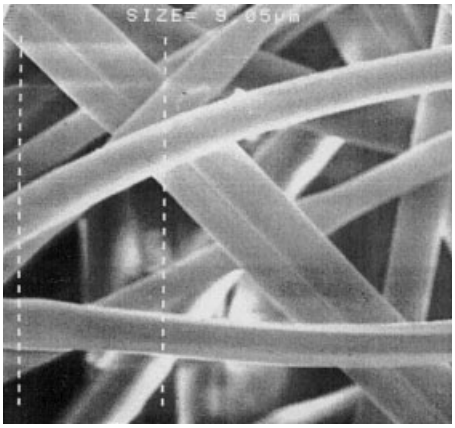

Figure 4 SEM image of Sample B (10 kV, 15 mmWD, ×3000).

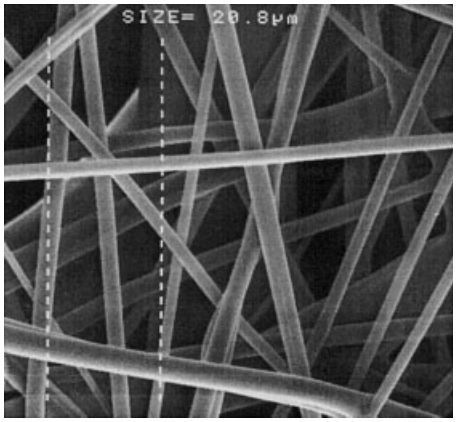

Figure 6 SEM image of Sample D (10 kV, 17 mmWD, ×2000).

etration test to visually inspect changes in the pore sizes attributed to the testing. Compared to the pore size distributions determined with the capillary porometer, pore sizes measured from SEM images do not result in real pore size distributions. They provide only an approximation of the average pore sizes. Apparently, the surface imaging is not an adequate way of describing the pore structure because it does not consider the bulk of the material. Porosities of the samples, however, were determined using the SEM images. An approximation of porosity was made based on these images. The pore sizes were used to estimate penetration pressures numerically and to compare with the experimental results; fabric thickness, porosity, and pore size distributions together were used to model the fabric structure, which will be presented in an upcoming report.

In addition to fabric parameters, several liquid parameters were also determined for comparison of numerically and experimentally determined penetration pressures and for liquid modeling. Distilled water was used for the penetration and flow tests. Water surface tension was determined before the penetration testing using a DuNoüy tensiometer (CSC Scientific Company, Inc., Fairfax, VA). The water viscosity was determined using a viscometer (Gilmont Instruments, Barrington, IL), which operates by measuring the rate of settling of a spherical ball. In addition, aliquots of the challenge liquid were obtained after the penetration/flow testing, and the surface tension and the viscosity measurements were repeated. The penetration/flow test had little or no effect on the surface tension and the viscosity of water. The water density was determined using a pycnometer.

Contact angles of all samples/solution combinations were determined using a dynamic contact angle analyzer (Cahn Instruments Corp., Madison, WI). It should be noted that these measurements were taken at the surface of the fabric; thus, the macroscopic contact angle is determined. It does not necessarily correlate with the microscopic contact angle inside the material's pores.

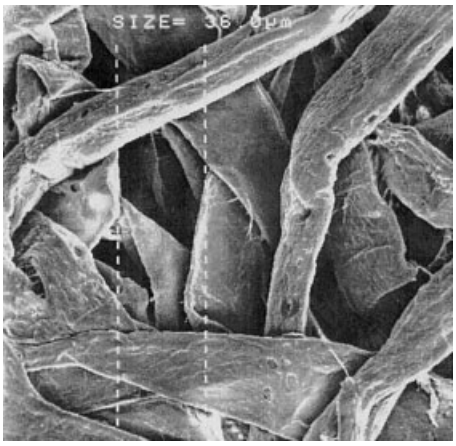

Figure 5 SEM image of Sample C (10 kV, 15 mmWD, ×450).

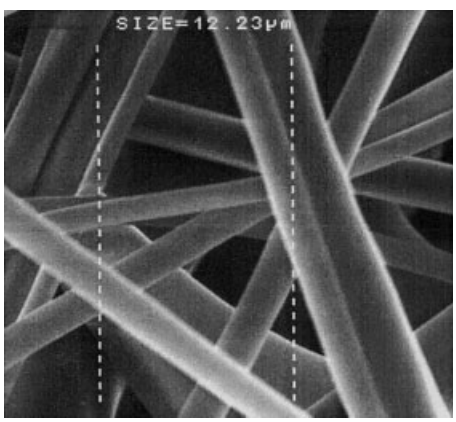

Figure 7 SEM image of Sample E (10 kV, 15 mmWD, ×3000).

Fluid penetration testing

As the air pressure in the reservoir and, consequently, the liquid pressure are increased, the liquid will at some point start to displace the air present in the largest pores of the fabric sample. The flowing liquid was subsequently collected in a beaker positioned on a balance (Fig. 2), and the mass of liquid per measured time was recorded. The pressure was then stepwise increased and for every applied pressure the flow rate was determined as water started to flow through additional (smaller) pores. The liquid pressure on top of the fabric at which the first liquid drops appeared at the bottom of the fabric sample was assumed to be the displacement pressure. The liquid pressure was increased in increments of 1 kPa until a preset maximum pressure was reached. The changes in liquid level in the supply bottle were accounted for in the calculation of the liquid pressure values on top of the fabric. Once the maximum preset pressure value was reached, the pressure was stepwise decreased in 1-kPa intervals to check for possible hysteresis in the flow rate–pressure relations.

Ink-bottle effect

The capillary pores in fabrics are composed of sections with different diameters. Consequently, each of these sections has a different displacement pressure, with the smallest sections requiring the greatest displacement pressure. To fill an entire sequence of sections with different diameters, the liquid pressure must exceed the smallest section's displacement pressure.

When the liquid pressure is being reduced, the smallest pores will lose their water first, followed by increasingly larger pores. The drainage of water from a pore with different sections is thus determined by the largest sections. As a result, pores with different sections will require greater pressures to fill with water than to drain, and consequently exhibit hysteresis.

Influence of metal screen

To determine the necessity of a supporting screen, an initial test was carried out with and without the supporting screen. Without the screen, penetration occurred at a lower pressure, whereas the flow rate was greater than that with the screen (Fig. 8). We concluded that sagging had occurred in the sample, which caused an increase in pore sizes. This was supported by SEM images.

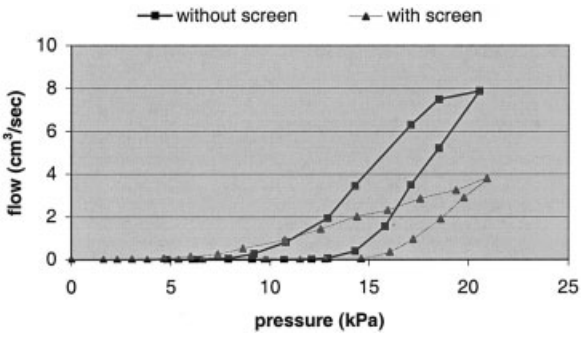

Figure 8 Effect of screen.

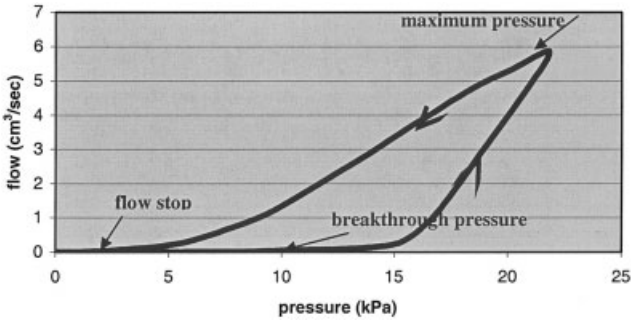

Figure 9 Typical plot of flow rate (water was applied to an initially dry fabric and pressure was stepwise increased to a maximum and stepwise decreased until the flow stopped).

Finally, we speculated that some of the hydrophobic polymeric materials might change their behavior to hydrophilic under prolonged contact with water.[1] Therefore, a sample of each fabric was submerged in water for 24 h and tested for possible changes. No significant changes in flow rate and only an occasional decrease in the breakthrough pressure were observed. The latter was attributed to some trapped water in the surface pores, and somewhat different pore sizes from sample to sample of the same type of material.

RESULTS AND DISCUSSION

Each test consisted of two parts during which the liquid pressure was first increased from a minimum to a maximum, and subsequently decreased until the cessation of water flow. It should be noted that, because the samples were all hydrophobic, air was the wetting fluid. During the increasing pressure of the first part, the challenge liquid was applied to dry fabric, and the starting pressure was 0 kPa (Fig. 9). We will refer to this as the initial displacement of air by water, or initial air drainage (IAD) phase. The liquid pressure was stepwise increased in 1-kPa intervals until 10 kPa beyond the breakthrough pressure. The second section of the first part, when the pressure was stepwise decreased in 1-kPa intervals until the flow stopped, was called the main displacement of water by air, or the main air wetting (MAW) phase (Fig. 9). It should be noted that the pressure value at which the water flow stopped was always lower than the pressure value at which it started (i.e., the penetration pressure). We suspected that the initial application of the challenge liquid under pressure caused some change in the pore alignment; some pores became

even larger, whereas the others became smaller. Consequently, the enlarged pores had lower displacement pressures. More important, however, water flow values during air wetting were higher than those during air drainage at corresponding pressure values, which is referred to as hysteresis. The hysteresis was attributed to (1) the pore sizes had increased by the initial application of the liquid, (2) the ink-bottle effect, (3) the contact angle effect, and (4) the presence of trapped liquid in the pores.

After the flow had stopped, the procedure was repeated. Thus, secondary air drainage and air wetting curves were established. It was observed that during the secondary displacement of air by water [main air drainage (MAD) phase], the flow values were higher than the initial flow values at the same pressures (Fig. 10). However, during the secondary displacement of water by air, the flow values were only slightly different, at the same pressures, from those during the initial wetting by air. This confirmed that some pore sizes increased during the initial penetration and remained the same thereafter. Consequently, the flow rate differences during wetting and drainage of air were now ascribed to changes in contact angle, the ink-bottle effect, and the entrapment of liquid.

Repeating the process of liquid wetting and drainage for a third time resulted in curves overlapping with the secondary curves (Fig. 11). This also confirmed that the pore sizes remained the same.

As seen from Figures 9 and 10, nonlinear relationships exist for parts of the curves between flow rate and pressure. The slope at any point of a curve represents the conductance C of the fabric.[15] From the Darcy equation

$$q = \frac{Q}{A} = -K\frac{\Delta H}{\Delta z} \tag{1}$$

where q is the Darcy flux (cm s^{-1}), Q is the volumetric flow rate (cm^3 s^{-1}), A is the cross-sectional area of fabric (cm^2), K is the hydraulic conductivity (cm s^{-1}), ΔH is the hydraulic head difference across the fabric

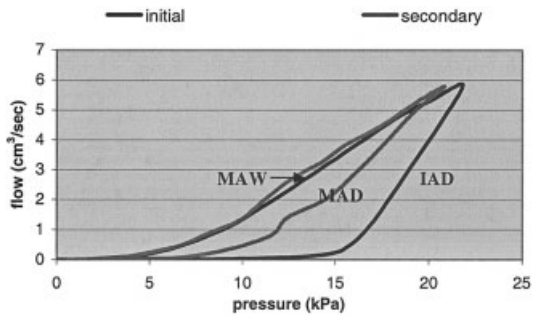

Figure 10 Typical plot of initial and secondary displacements for Sample A.

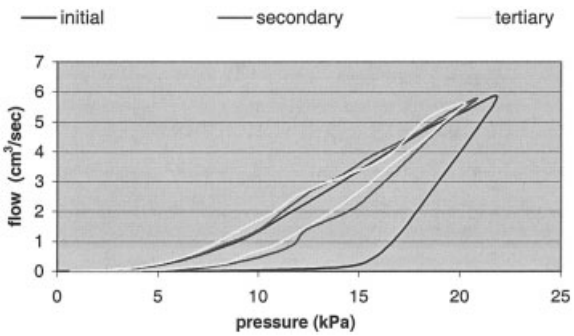

Figure 11 Plot of data first, second, and third parts for Sample A.

(cmH_2O), and Δz is the thickness of the fabric (cm). It follows that

$$Q = -C\,\Delta H \tag{2}$$

where

$$C = KA/\Delta z \tag{3}$$

When the flow first starts, only the largest pores conduct water; as the pressure increases, smaller pores also contribute to the liquid flow. Consequently, the conductance should increase as the pressure increases. When the flow rate–pressure curve becomes linear, the conductance is constant, and no additional pores are filled. At this point, the flow increases only because the pressure increases. For example, Figures 8, 9, and 10 show linear relationships for the IAD for pressures greater than about 18 kPa. Thus all pores are filled with water from this pressure on.

The experimental data can be used inversely to estimate pore size distribution. When the medium is dry, it is saturated with air. Once the liquid is forced into the medium, it starts to displace air in the pores. The pores with the largest diameters have the lowest displacement pressures; they are the first ones to be filled with water. Using the pressure value at which liquid first enters the medium allows the diameter of the largest pores to be calculated. As the pressure increases smaller and smaller pores start to fill with liquid, and consequently the conductance increases somewhat until the pressure–flow rate curve becomes linear, and all pores are filled. Using the pressure applied at the point where linearity begins, the diameter of the smallest pores can be determined. Thus, the nature of the pore size distribution can be estimated from the shape of the curve. The Young–Laplace equation was used to determine displacement pressures, as follows:

$$P_c = \frac{2\gamma\cos\theta}{r} = P_{\text{liquid}} - P_{\text{air}} \quad (P_{\text{liquid}} > P_{\text{air}}) \tag{4}$$

where P_c is the capillary pressure (Pa), γ is the liquid surface tension (N/m), θ is the gas/material contact angle, and r is the pore radius (m). The Poiseuille equation was used for flow rate calculations.

$$Q = \frac{\pi}{8\tau\eta}\frac{\partial P}{L}\sum_{i=0}^{n} r_i^4 \quad (5)$$

where Q is volumetric flow rate (m^3/s), r is the pore radius (m), P_0 is the liquid pressure at the beginning of the capillary (Pa), P_1 is the liquid pressure at the end of the capillary (Pa), τ is the tortuosity factor, η is the liquid viscosity (Pa s^{-1}), and L is the capillary length (m).

An estimated pressure–flow rate curve can be formed based on estimated pore size values. The actual and estimated pressure–flow rate curves can be compared to determine how accurate the estimated pore size distribution is. Therefore, an optimization process can be developed to obtain the best possible estimated pore size distribution. Considering Figure 9 (Sample A), we note that the flow started at approximately 11 kPa. This coincides with water entering the largest pores. The surface tension of water was determined as 0.072 N/m (72 dyn/cm), and the solid–liquid phase contact angle was measured as 120° (cos 120° = −0.5). Using the Young–Laplace equation, the largest pore diameter was determined to be 13 μm. According to the pore size distribution determined using the capillary flowmeter, Sample A had a diameter of 14.48 μm for its largest pores (Table I). A similar calculation was made to determine the smallest pore size. Note that the curve becomes linear at around 18 kPa (Fig. 9). Using the same values for the contact angle and surface tension in the Young–Laplace equation, the smallest pore diameter was determined to be 8 μm. The slope of the curve exhibits its greatest rate increase near 15 kPa, indicating that most of the pores are filled at this pressure. The corresponding pore diameter for this pressure is 9.5 μm.

CONCLUSIONS

In this study, a method for studying the wetting and drainage behavior of nonwoven, hydrophobic fabrics was presented. The liquid was applied to the top of the fabric under a sequence of increasing and decreasing pressures. The breakthrough pressure was determined as the pressure value at which the first liquid drops appeared at the bottom of the fabric. After the penetration pressure was reached, the liquid pressure was incremented in steps of 1 kPa until a preset maximum pressure, and subsequently decreased until the flow stopped. The flow rates were determined at each pressure step. Different flow rates were observed during increasing and decreasing liquid pressures. This observed hysteresis was attributed to the ink-bottle effect, trapped liquid in the pores, and variation in contact angle. In addition, the following observations were made:

- Pore sizes increase during the initial air drainage.
- Flow rate increases as pressure increases.
- Initially, a nonlinear relationship exists between the flow rate and the liquid pressure. When all pores have become water filled, this relationship becomes linear.
- More pores are filled as the liquid pressure increases; consequently, the hydraulic conductance increases as more pores are filled.
- It is possible to determine the pore size distribution of the material from the flow rate/liquid relation.
- Pressure at penetration is strongly dependent on the pore sizes of the material.

Even though other investigators have studied liquid penetration into fabrics, most of them considered hydrophilic textiles. Our methodology offers insight into the penetration of liquid into and subsequent flow in hydrophobic textiles. Liquid parameters, such as surface tension, viscosity, and contact angle, have substantial effects on the penetration pressures and flow rates. All these effects will be the focus of a subsequent report.

References

1. Miller, B.; Tyomkin, I. Text Res J 1984, 54, 706.
2. Thiry, M. C. AATCC Rev 2003, 9.
3. Minor, F. W.; Schwartz, A. M.; Wulkow, E. A.; Buckles, L. C. Text Res J 1959, 29, 940.
4. Minor, F. W.; Schwartz, A. M.; Buckles, L. C.; Wulkow, E. A.; Marks, M. P.; Fielding, G. H. Text Res J 1961, 31, 525.
5. Miller, B.; Clark, D. B. Text Res J 1978, 48, 150.
6. Miller, B.; Clark, D. B. Text Res J 1978, 48, 256.
7. Miller, A.; Schwartz, P. Text Res J 2000, 70, 77.
8. Minor, F. W.; Schwartz, A. M.; Wulkow, E. A.; Buckles, L. C. Text Res J 1959, 29, 931.
9. Miller, B.; Young, R. A. Text Res J 1975, 45, 359.
10. Trevino, L.; Rupel, K.; Young, W. B.; Liou, M. J.; Lee, L. J. Polym Compos 1991, 12, 20.
11. Coulter, J. P.; Guceri, S. I. Compos Sci Technol 1989, 35, 317.
12. Adams, K. L.; Miller, B.; Rebenfeld, L. Polym Eng Sci 1986, 26, 1434.
13. Koorevaar, P.; Menelik, G.; Dirksen, C. Elements of Soil Physics; Elsevier: Amsterdam, 1983; pp. 1–3.
14. ASTM D 1777-96. Annu Book ASTM Stand 1996.
15. Leonarmand, R.; Toubul, E.; Zarcone, C. J Fluid Mech 1988, 189, 165.